INVESTIGATION OF OXIDE STRENGTHENED STEELS PREPARED BY POWDER METALLURGY

Cs. Balázsi[1], Gy. Török[2], F. Gillemot[2], M. Horváth[2], F. Wéber[1], F. Cinar Sahin[3], Y. Onüralp[3], G. Göller[3], L. Tatár[2], and A. Horváth[2]

[1] Ceramics and Nanocomposites Department, Research Institute for Technical Physics and Materials Science, Konkoly-Thege M. 29-33, 1121 Budapest, Hungary
[2] KFKI Atomic Energy Research Institute, Konkoly Thege M. 29-33, 1121 Budapest, Hungary
[3]Metallurgical and Materials Engineering Department, Istanbul Technical University, 34469 Maslak Istanbul, Turkey

Abstract

Future nuclear reactors are designed to operate at significantly higher temperature than the present fleet of light water reactors. In addition, most of the advanced design concepts have higher anticipated radiation damage levels. Nanoscale modifications of the existing strengthened steels offer the best opportunity to improve the radiation resistance and allowable operating temperature window for structures. Homogeneous dispersion of nanosize oxide particles in the metal matrix promotes recombination of point defects and mitigates swelling caused by helium. Although the capability of steels has been improved in the past by thermomechanical treatment, utilization of powder metallurgy provides with more controlled microstructure and tailored properties in terms of strength and radiation resistance. For further improvement of the superior mechanical properties, fundamental understanding of the influence of composition and heat treatment on the microstructural development is necessary. The paper summarizes recent results on Oxide Dispersion Strengthened, ODS steel development.

Keywords: strengthened steel, nanostructured ODS steel, attritor milling, neutron irradiation

1. Introduction

Advanced nuclear energy systems proposed under the Generation IV initiative are aimed at making revolutionary improvements in economics, safety and reliability, and sustainability. To achieve these advancements, Generation IV systems anticipate operating at much higher temperatures and to higher radiation damage than current light water reactors. Of the candidate alloy systems being considered, ferritic–martensitic alloys are expected to play an important role as cladding or structural components in Generation IV systems operating in the temperature range 350–700 °C and to doses up to 200 dpa [1-4].

As one of the Generation IV nuclear reactors, a supercritical water cooled reactor (SCWR) is being considered as a candidate due to its high thermal efficiency and simple reactor design without steam generators and steam separators [5,6]. At above the supercritical condition of 374 °C, 22.1 MPa, the supercritical water does not change its phase through out the reactor core outlet. Therefore, the high temperature coolant is effectively used at over 40% thermal efficiency [7–9].

Oxide dispersion strengthened ferritic-martensitic steels are applicable not only as long-life cladding materials in fast reactors, but also as fusion reactor materials due to their excellent properties [10]. ODS ferritic alloys containing a high number density of small oxide particles have been investigated for use as fuel cladding and structural applications in nuclear systems for several decades, not only because of they have excellent high temperature tensile properties and creep resistance, but because the particles also increase the alloy's resistance to radiation-induced changes in mechanical properties and swelling [11,12].

ODS steels have attracted attention for advanced nuclear power plants applications such as fast and fusion reactors, because of their superior high temperature mechanical properties. They are being developed and investigated for nuclear fission and fusion applications in Japan (JNC) [13,14], Europe [15,16], and the United States [17,18]. Since earlier JNC-developed ODS ferritic steel claddings had strong anisotropy in their mechanical properties and low elongation in the hoop direction at around 673 K due to strong microstructural anisotropy [19], recrystallization and a–c phase transformation procedures have been applied in the tube manufacturing process of newer ODS ferritic/martensitic steel claddings in order to improve microstructural anisotropy and to allow manufacturing of cladding tubes by the cold-rolling technique [20].

The European reference RAFM steel is denominated EUROFER; its nominal composition is 8.9Cr, 1.1W, 0.2V, 0.14Ta, 0.42Mn, 0.06 Si, 0.11 C and Fe for the balance [21]. This steel was chosen for the production of two variants of ODS steels with different Y_2O_3 contents (0.3% and 0.5%), which should allow a substantial increase of about 100 °C for the operating temperature. Activation calculations showed that addition of yttria would not impair long-term activation properties. Early versions of EUROFER ODS were manufactured by inert gas atomisation of EUROFER by STARCK, followed by mechanical alloying in industrial ball mills of attritor type by PLANSEE.

Powder metallurgy (PM) of stainless steel components constitutes an important and growing segment of the PM industry. Mechanical alloying and powder metallurgy processes are applied to finely disperse these small oxide particles in the matrix, because oxide particles

aggregate together and coarsen during conventional casting processes. The PM processing provide a feasible and economic manufacturing of austenitic stainless steels components with complex shape and advantages such as good dimensional precision, high surface finish and good mechanical properties [22,23]. However, corrosion resistance of sintered stainless steels is lower than that of either cast or wrought stainless steel; the inherently residual open porosity being mainly responsible for this behaviour.

This paper summarizes the results of development and structural studies of ODS steels prepared by powder metallurgy, especially by attritor milling.

2. Experimental

2.1. Preparation of oxide dispersion strengthened steels

Samples were prepared from pre-alloyed, commercial austenitic ODS-316 („Metco 41C" Fe, 17Cr, 12Ni, 2.5Mo, 2.3Si, 0.1C, AISI Type 316 stainless steel, water atomized, particle size: -106+45 μm) and martensitic ODS-431(„Metco 42C" Fe, 16Cr, 2Ni, 0.2C, AISI Type 431 stainless steel, water atomized, -106+45 μm) powders. As oxide addition, 1wt% Y_2O_3 with mean particle size 700 nm and particle size distribution (D90% 1.6 μm, D50% 700 nm, D10% 300 nm) was added to the steel powders. An efficient dispersion of ODS steels was achieved by employing a high efficient milling process, namely attritor milling (Fig. 1). In this proposal the dry and wet coating process of fine ceramic particles is proposed by the help of mechano-chemical processes assured by attrition milling. For some of the powder mixtures a high efficient attritor mill (Union Process, type 01-HD/HDDM) was employed. This apparatus allowed a higher rotation speed and a contamination free mixing process, because of ceramic (silicon nitride, zirconia) parts (tank, arm, balls) as shown in Fig. 1.

For composite processing the Field Activated Sintering method was used. This technique has a high potential to process bulk nanomaterials with good interparticle bonding [24-26]. The external field application is capable to induce fast densification and reasonable control of grain growth during sintering of ceramics when starting with nanocrystalline powders. The FAST method, in which the ceramic powder is annealed at lower temperatures and for much shorter times than other sintering processes (hot pressing (HP), hot isostatic pressing (HIP), pressure-less sintering (PLS)), allows the fabrication of fully dense ceramics and composites with a nanocrystalline microstructure. The electrical field activation has been pioneered by Taylor, who used resistance heating for hot pressing cemented carbides in 1933 [27]. In late 50's, resistance sintering under pressure was applied to metal powders by Lenel using an

equipment similar to spot welding [28]. Presently, resistive hot pressing is commonly used and consists of a low-voltage (5-40 V), high-amperage (up to 25 kA) current passing through the powders with a simultaneous pressure application. The main difference between FAST and hot pressing is the simultaneous application of a pulsed current in the former, which generates electrical discharges [29]. The electrical discharges do not densify powders and, therefore, additional energy is required to increase the final density. This extra energy may be mechanical, as an applied pressure, and thermal by generating higher temperatures than that created by electrical discharge.

Fig. 1 . *The design of the highly efficient Szegvari type attritor mill.*

Electrical current activation has been applied in the plasma assisted sintering (PAS) process developed in Japan in the 60's, followed by the presently largely used spark plasma sintering (SPS) [30]. Field sintering techniques are also known as instrumented pulse electro-discharge consolidation, pulsed electric current sintering, resistance/spark sintering under pressure, pulsed electrical discharge with pressure application, high energy high rate processing or pressure plasma sintering. All these methods are essentially identical in the application of a pulsed discharge and subsequent or simultaneous resistance sintering. The pulsed electro-discharge stage may be built-in as an added option for powder activation in other non-field sintering techniques, such as the piston-cylinder high pressure method [31]. These techniques

are different from other electrical field assisted sintering methods such as electrodischarge compaction (EDC) [31].

A set of composites were sintered by the help of spark plasma sintering, with the system capacity 10 V and 20.000 amper from Sojitz Japan, Dr.Sinter-SPS-7.40MK-VII. The sintering was performed in vacuum, at 50 MPa mechanical pressure, 940-950°C temperature and 5 min. dwelling time. Circular samples with 50 mm were realized. This samples have been cut by diamond wheels to bars with rectangular geometry. The density of the sintered materials was measured by the Archimedes method. Three point bending strength was determined on Instron testing machine. Microhardness was calculated by applying 5N and 10N loads.

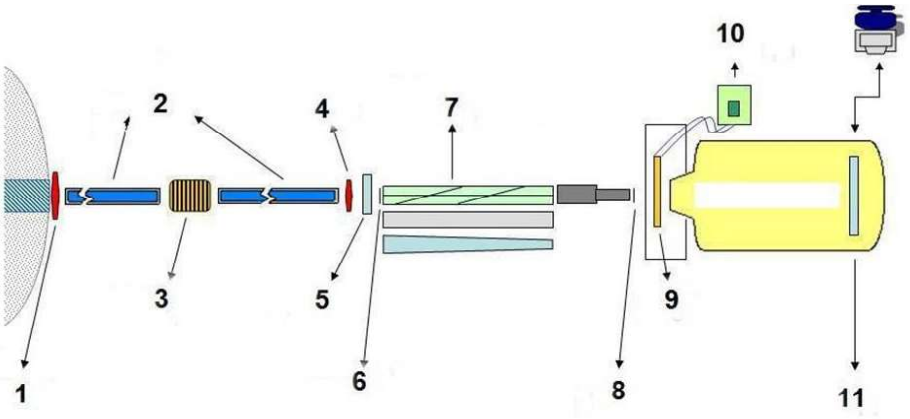

Fig. 2. *Layout of the SANS instrument (1, 4 – beam shutters, 2 – neutron guides; 3 – velocity selector; 5,6,8 – diaphragms; 7 – movable collimator (neutron guide); 9 – sample shielding; 10 –temperature control; 11 – detector, 12 shield behind the detector)*

2.2. Measurement methods

The morphology and microstructure of the powder and the sintered steels were studied by scanning electron microscopy. Phase compositions were determined by an X-ray diffracto-meter with CuKα radiation. The mechanical strength at room and high temperatures (500 C), as well as Vickers hardness of the samples were also measured.

Small Angle Neutron Scattering measurements (SANS) were performed in the Measurement Hall at the Budapest Neutron Center. The layout of the instrument is shown in Fig 2. The machine is equipped with a 64x64 cm^2 BF_3-detector, the sample-detector distance is variable between b=1.3-5.5 m. The wavelength λ=0.3-2.4 nm is selected by mechanical velocity selector, width $\Delta\lambda/\lambda$=0.13. The measurements were executed in momentum transfer range q = 0.1–4 nm^{-1}. By changing the wavelength and sample–detector distance, we have covered the range R~1/q~0.3–10 nm of nanodefects.

Residual stresses can be introduced into engineering components during manufacture as a result of, for example, forging, bending and welding processes. Stresses (or strain) were

measured in radial, hoop and axial directions at Athos spectrometer, with gauge volume less than 5x5x5 mm. The arrangement of spectrometer for residual stress was proven in a previous Round Robin experiment coordinated by IAEA. The reason is the highly preferred orientation at direction 111 and multiple scattering in the depth of sample. The JRC measurement was carried out at different wavelengths.

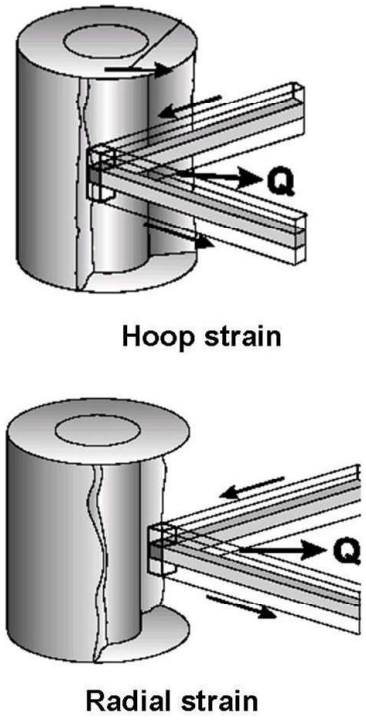

a) b)

Fig. 3. *Measurement of residual stresses. a) Experimental setup, b) Radial and hoop strain measurement positions.*

3. Results and discussion

3.1. Structural characterization

The SEM investigation of the starting ODS powders showed non-regular austenitic and martensitic structures (Fig. 4). The mean grain size was about 100 μm for both samples. The compositions of basic powders were different from that given by the producer. The austenitic steel powder was comprised of 17 wt% Cr, 12 wt% Ni, 2.5 wt% Mo, 2.3 wt% Si and 0.1 wt%

C next to iron. The martensitic steel powder consisted of Fe with 16 wt% Cr, 2 wt% Ni, and 0.2 wt% C.

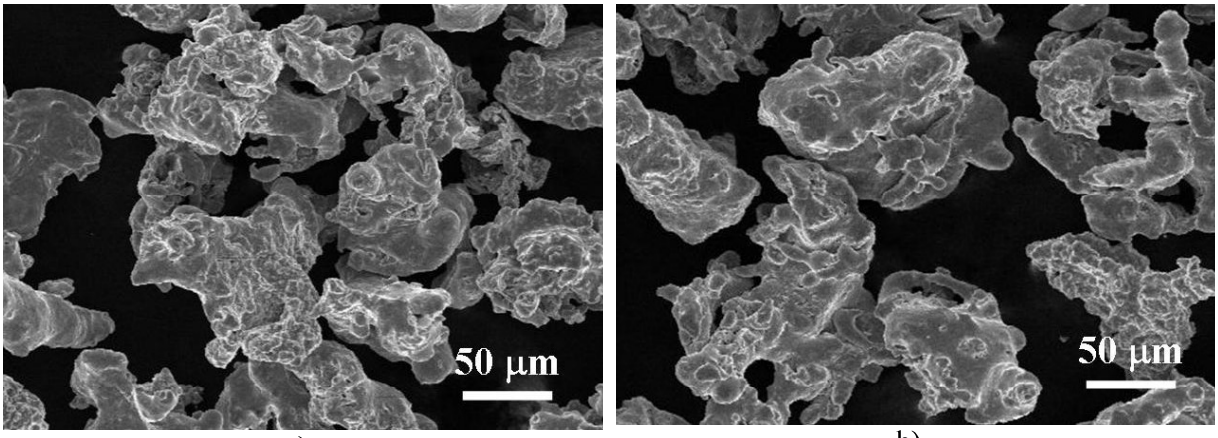

a) b)

Fig. 4. *SEM images of commercial steel powders. a) austenitic, b) martensitic.*

The attritor milling process consisted of 5 hours wet milling in ethanol at 600 rpm. The structure of powders considerably changed after intensive milling as shown in Figs. 5 – 8. The grain size of austenitic ODS powder with Y_2O_3 addition is between 2 and 50 microns in average, however the grains are sticked to 5 and 20 microns grains presenting a non-regular morphology (Fig. 5). Lamellar shaped grains may be observed. EDS analysis of the milled austenitic ODS/Y_2O_3 reveals the homogeneous dispersion of Y_2O_3 addition in steel matrix (Fig. 6).

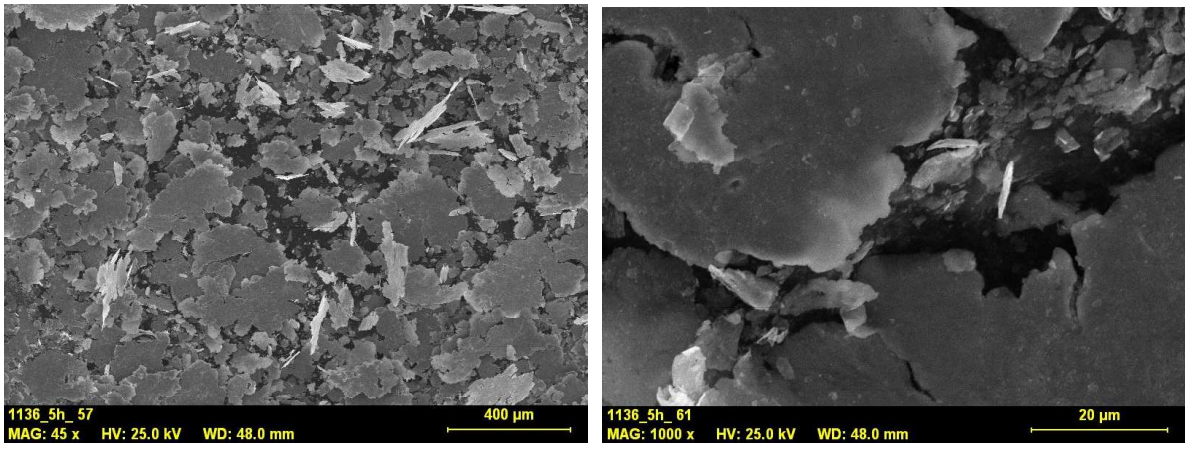

a) b)

Fig. 5. *SEM images of milled austenitic sample with 1 wt% Y_2O_3 addition. a) low magnification, b) high magnification*

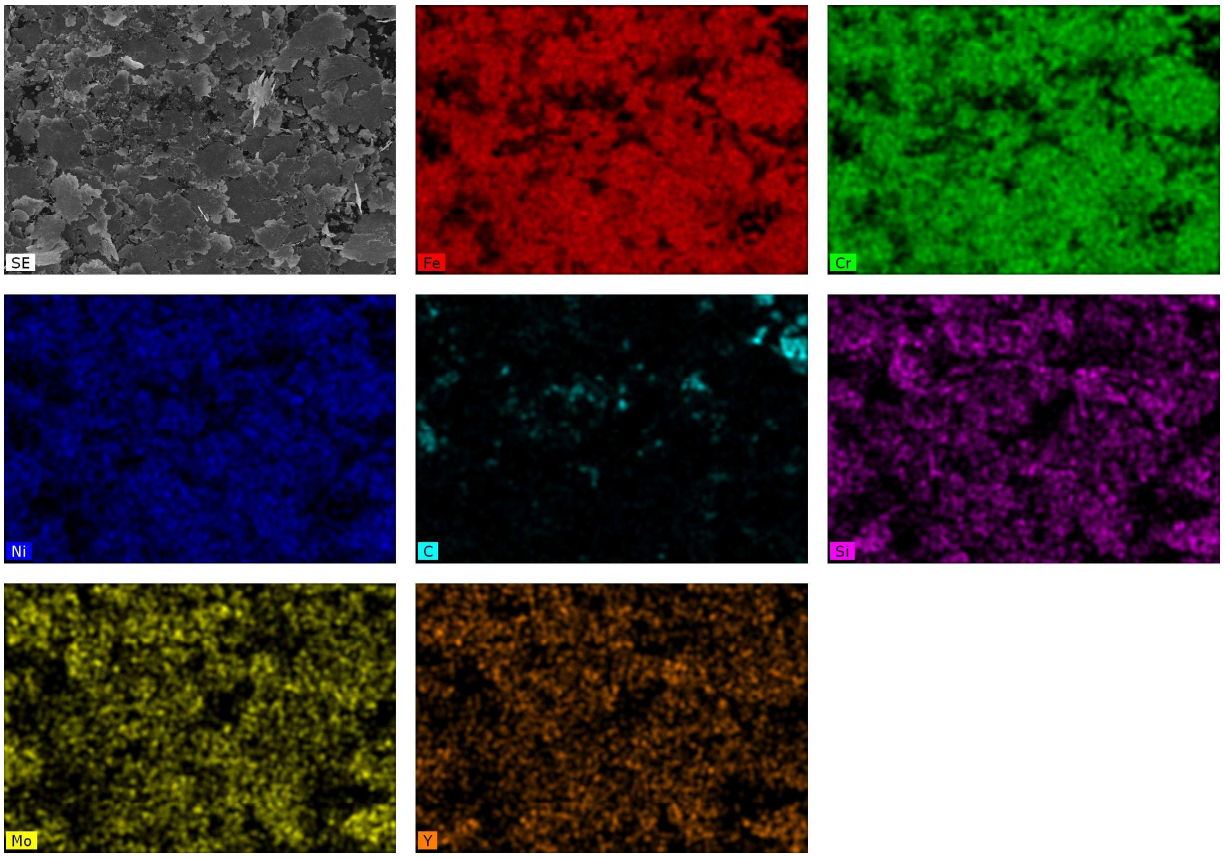

Fig. 6. *Map of elemental composition of a milled austenitic sample with 1 wt% Y_2O_3 addition.*

The martensitic ODS powder grain size is considerably lowered compared to that of the starting powder (Figs. 7 and 8). The grain size of martensitic ODS/Y_2O_3 is between 30 and 50 microns in average, however these grains are sticked to 5 and 20 microns grains presenting a non-regular morphology (Fig. 7).

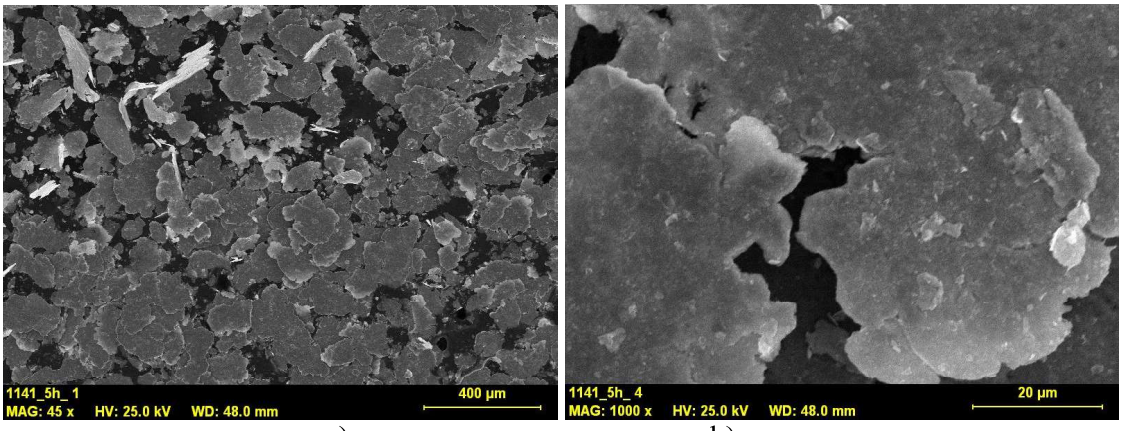

a) b)

Fig. 7. *SEM images of milled martensitic sample with 1% Y_2O_3 addition. a) low magnification, b) high magnification*

As in the case of austensitic ODS, lamellar shaped grains are observed. The EDS analysis of milled martensitic ODS/Y_2O_3 shows homogeneous dispersion of the addition in steel matrix (Fig. 8).

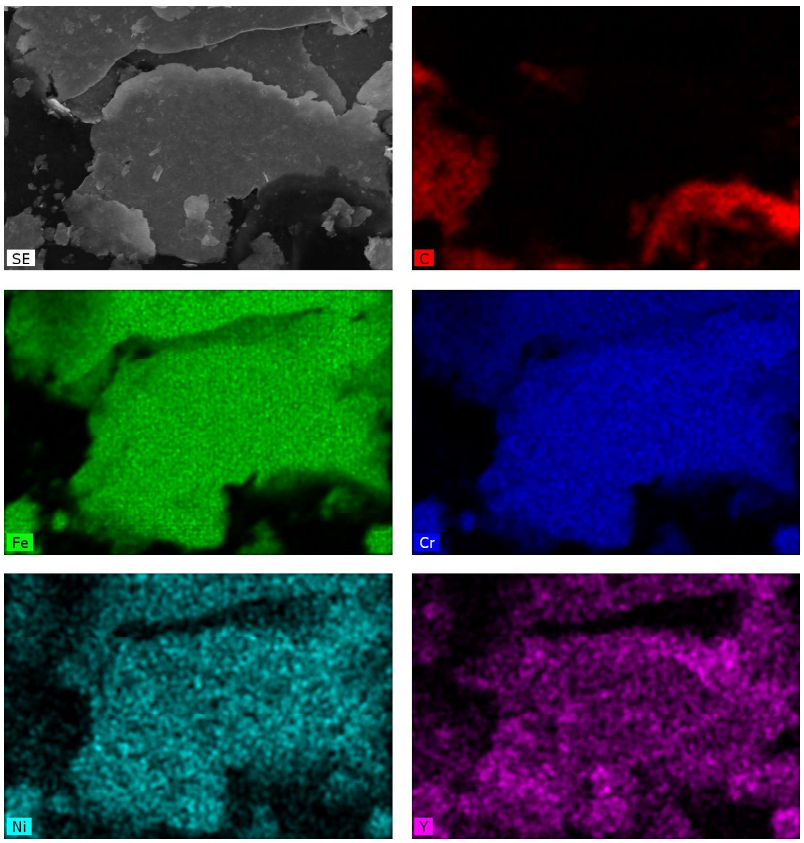

Fig. 8. *Map of elemental composition of milled martensitic powder with 1% Y_2O_3 addition.*

By using the SPS method densification of samples without considerable grain growth can be achieved within few minutes (Fig. 9). Fracture surfaces of ODS samples prepared by SPS are presented in Fig. 10. Grains with 300 nm mean size may be found in both cases.

The ODS steel samples after fabrication were investigated with SANS (Fig.11). The results were interpreted supposing isotropic behaviour and fractal structure at the grain boundaries. The aim of the investigation was to find correlation between the calculated fractal dimension and the mechanical properties. The fractal dimension was calculated as the slope of the fitted linear section of the normalised scattered intensity. The summary of the fractal dimensions for the samples investigated is shown in Tab. 1. Fractal dimension should be correlated to the compliance of the samples in a mechanical loading test. The ODS steel samples were found to be brittle during the mechanical testing, and the correlation between the strength or hardness could be hardly seen.

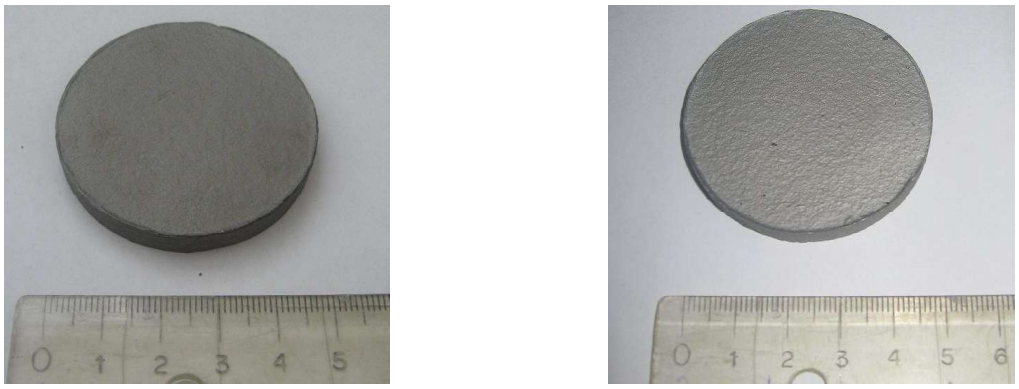

a) b)

Fig. 9. *Macroscopic view of sintered ODS samples. a) austenitic ODS, b) martensitic ODS.*

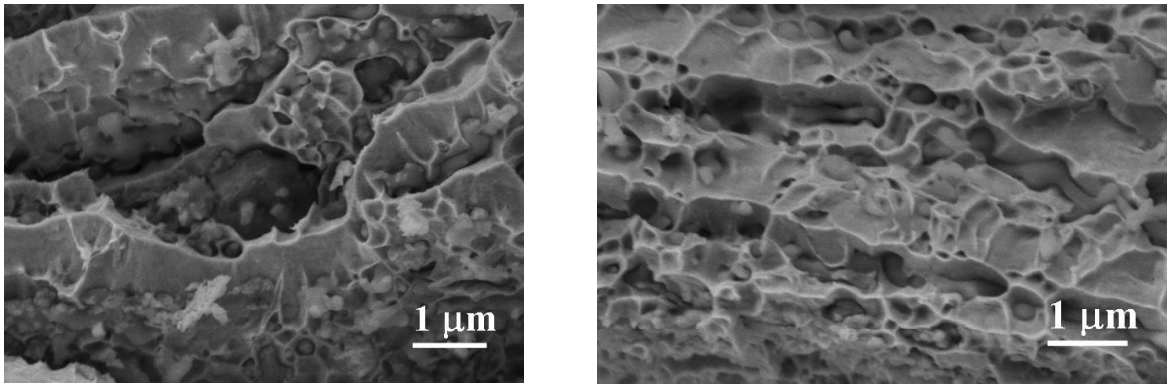

a) b)

Fig. 10. *SEM images of fracture surface of sintered ODS. a) austenitic ODS with 1 wt% Y_2O_3 addition, b) martensitic ODS with 1 wt% Y_2O_3 addition.*

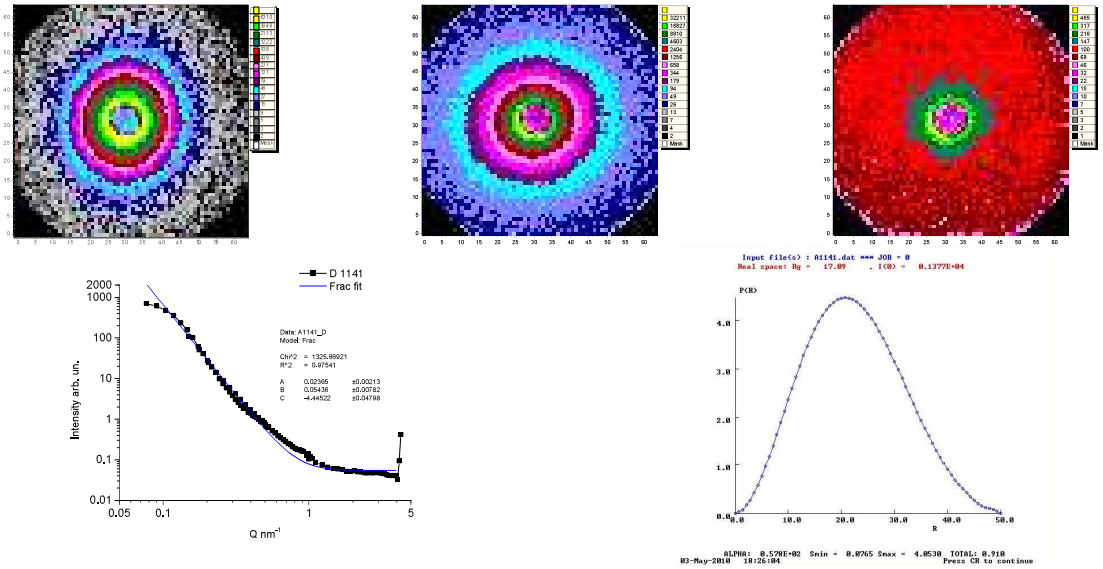

a) b)

Fig. 11. *SANS results of martensitic sample. a) Normalised scattered intensity, b) Particle correlation length distribution*

Sample	Fractal dimension
Martensitic ODS +1 wt%Y_2O_3	2.298
Austenitic ODS +1wt% Y_2O_3	2.213

Tab. 1. *Fractal dimension derived from the normalised scattered length of different ODS steel samples. SANS measurement performed at BNC, neutron wavelength λ=0.4 nm.*

The SANS investigation of the samples will continue with irradiated steel probes. In order to be able to handle activated material, an additional gamma shielding is designed for the instrument. The irradiated small samples will be put in a shielded box in the hot cell, and transported to the Cold Neutron Hall. The maximal expected dose of the sample measured at 1 m distance is 100 μSv/h. This translates to $E_{max} = 10^{-4}$ J / kg/ h, so the shielding is designed accordingly. As the maximum weight is 1000 kg which can be mounted on the sample holder, the thickness of the lead shielding can only be 5 cm.

3.2. Mechanical characterization

Microhardness of sintered ODS was measured with 10N load (Tab. 2). Obviously, the microhardness of ODS (martensitic) ferritic steels are higher than that of ODS austenitic steels. The hardness of ODS steels sintered by SPS is much higher than that of steels sintered by HIPing [32]. This may be because of the very fast sintering speed and very short sintering time of SPS compared with HIPing, which leads to a much finer grain size of SPS-ODS steels than that of ODS steels by HIPing.

Sample	HV (10 N)	Rm, MPa 20 °C	Rm, MPa 500 °C
ODS martensitic + 1 wt%Y_2O_3	592	780	697
ODS austenitic + 1wt% Y_2O_3	389	677	463

Tab. 2. *Hardness (HV) and strength (Rm) of different ODS steel samples. Strengths are measured at room temperature and at 500 °C.*

The bending strength-strain curves related to sintered austenitic and martensitic ODS are presented in Fig. 12. A brittle behaviour is shown in both cases. Bending strength as high as ~1690 MPa was found for martensitic ODS, whereas ~ 1385 MPa for austenitic ODS.

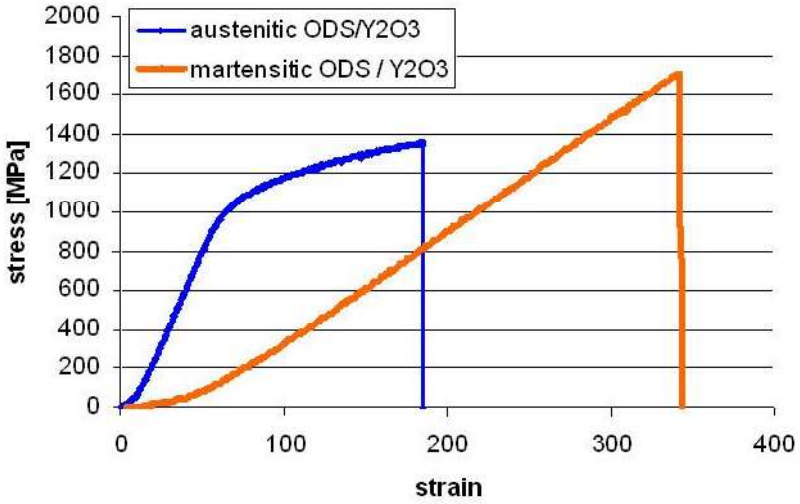

Fig. 12. *Strength – strain curves of sintered austenitic and martensitic ODS samples.*

3.3. Measurement of residual stresses in welded structures

Residual stresses can be introduced into engineering components during manufacture as a result of, for example, forging, bending and welding. They can also be caused by the forces and thermal gradients imposed during operation. These stresses can affect the load-carrying capacity and resistance to fracture of components. In order to quantify their effect it is necessary to know their magnitude and distribution (Fig. 13).

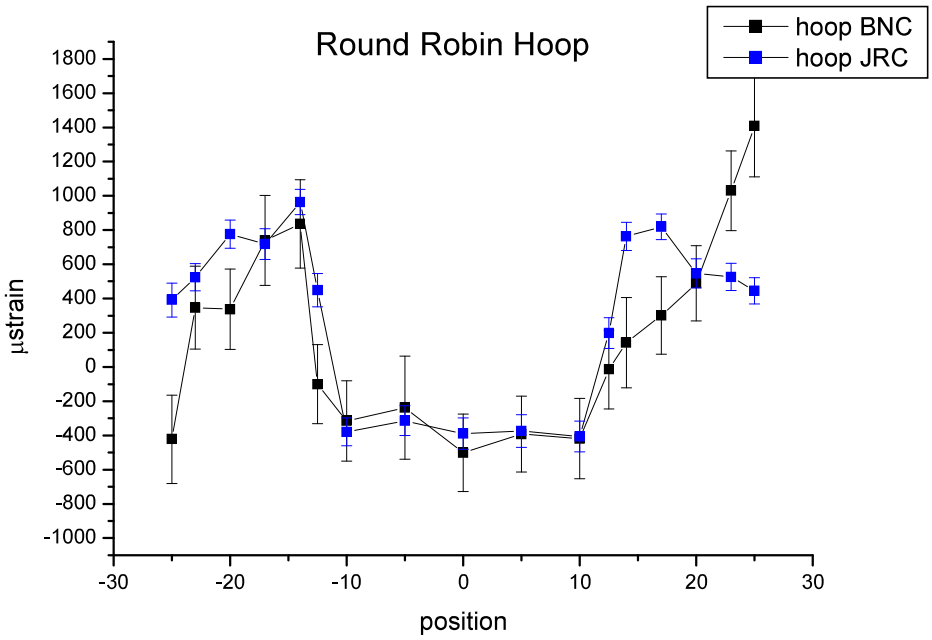

Fig. 13. *The comparison of hoop microstrain results with the data measured at JRC-IE on the same probe (IAEA CRP 1314 on „Development and Applications of the Technique of Residual Stress Measurement in Materials")*

4. Conclusion

This paper summarizes recent results of structural studies and mechanical testing of oxide dispersed steel (ODS) samples. The structure of powders considerably changed after intensive milling. The grain size of ODS powders was around 20-50 microns in average, however this grains were stacked to 5-20 microns grains presenting a non-regular morphology in the same time. Sintering of ODS powders was performed by spark plasma sintering. Grains with 300 nm mean size have been found in austenitic ODS. In comparison the martensitic ODS microstructure consisted of grains with 200-300 nm in size. The ODS steel samples were found to be brittle during mechanical testing, and the correlation between the strength or hardness could be hardly seen. The martensitic ODS had almost double hardness than austenitic ODS.

Acknowledgements

This work was supported by EFDA, FEMAS. The help in the preparation of this work is gratefully acknowledged to P. Koncz, V. Varga, A. Petrik, L. Illés from MTA-MFA.

References

[1] A Technology Roadmap for Generation IV Nuclear Energy Systems, GIF-002-00, US DOE Nuclear Energy Research Advisory Committee and the Generation IV International Forum, December 2002.
[2] S.J. Zinkle, L.J. Ott, D.T. Ingersoll, R.J. Ellis, M.L. Grossbeck, in: M.S. El-Genk (Ed.), Proceedings of Space Technology and Applications International Forum, STAIF-2002, AIP Conference Proceedings 608 (1), American Institute of Physics, NY, 2002, p. 1063.
[3] D.S. Gelles, DOE/ER-0313/16, March 1994, p. 146.
[4] S. Yamashita, K. Oka, S. Ohnuki, N. Akasaka, et al., J. Nucl. Mater. 307–311 (2002) 283.
[5] K. Kataoka et al., in: Proceedings of ICAPP 03, Cordoba, Spain, 4–7 May, 2003.
[6] D. Squarer, T. Schulenberg, D. Struwe, Y. Oka, D. Bittermann, N. Aksan, C. Maraczy, R. Kyrki-Rajamaki, A. Souyri, P. Dumaz, Nucl. Eng. Des. 221 (2003) 167.
[7] Y. Oka, S. Koshizuka, SCR-2000, 6–8 November 2000, Tokyo, The University of Tokyo, 2000, p. 1.
[8] J. McKinley, S. Teysseyre, G.S. Was, D.B. Mitton, H. Kim, J.-K. Kim, R.M. Latanision, GENES4/ANP2003, 15–19 September, 2003, Kyoto, Japan, Paper No. 1027.
[9] G.S. Was, S. Teysseyre, J. McKinley, in: NACE's International Conference, Corrosion

2004, New Orleans, Paper No. 04492, 2004.
[10] D.K. Mukhopadhyay, F.H. Froes, D.S. Gelles, J. Nucl. Mater. 258–263 (1998) 1209.
[11] J.J. Huet, Powder Metall. 10 (1967) 208.
[12] J.J. Huet, V. Leroy, Nucl. Tech. 24 (November, 1974) 216.
[13] S. Ukai, T. Nishida, H. Okada, T. Okuda, M. Fujiwara, K. Asabe, J. Nucl. Sci. Tech. 34 (1997) 256.
[14] S. Ukai, T. Yoshitake, S. Mizuta, Y. Matsudaira, S. Hagi, T. Kobayashi, J. Nucl. Sci. Technol. 36 (1999) 710.
[15] A. Alamo, J. Decours, M. Pigoury, C. Foucher, Structural Applications of Mechanical Alloying, ASM International, Materials Park, OH, 1990.
[16] A. Alamo, H. Regle, G. Pons, L.L. Bechade, Mater. Sci. Forum 88–90 (1992) 183.
[17] D.K. Mukhopadhyay, F.H. Froes, D.S. Gelles, J. Nucl. Mater. 258–263 (1998) 1209.
[18] M.K. Miller, E.A. Kenik, K.F. Russell, L. Heatherly, D.T. Hoelzer, P.J. Maziasz, Mater. Sci. Eng. A 353 (2003) 140.
[19] S. Ukai, M. Fujiwara, J. Nucl. Mater. 307–311 (2002) 749.
[20] R. Lindau et al., *Present Development Status of EUROFER and ODS-EUROFER for Application in Blanket Concepts*, Fusion Engineering and Design 75-79 (2005), 989-996.
[21] F. Borgioli, E. Galvanetto, T. Bacci, et al., Surf. Coat. Technol. 149 (2002) 192–197.
[22] O. Sandberg, L. Jönson, Advances in Powder Metallurgy, Adv. Mater. Process. 12 (2003) 37–42.
[23] P. Lindskog, The future of ferrous PM in Europe, Powder Metall. 47 (2004) 6–9.
[24] M. Palm, J. Preuhs, G. Sauthoff, Production scale processing of a new metallurgical NiAl-Ta-Cr alloy for high-temperature application. PART II., Powder metallurgical production of bolds by HIP, J. Mater. Process. Technol., 136, 2003, 114-119
[25] J. R. Groza, S. H. Ribaud, K. Yamazaki, Plasma Activated Sintering of Additive free AlN Powders to Near-theoretical Density in 5 Minutes, J. Mater. Res. 7 (1992) 2643-45.
[26] J. R.- Groza, J. D. Curtis, M. Kramer, Field Assisted Sintering of Nanocrystalline Titanium Nitride, J. Am. Ceram. Soc. 83 (2000) 1281-83.
[27] J. R. Groza, A. Zavaliangos, Nanostructured bulk solids by field activated sintering, Review in Advanced Materials Science RAMS, ed I. Ovidko, St. Petersburg.
[28] G. F. Taylor, US Patent No. 1,896,854, Feb 7,1933.
[29] F. V. Lenel, JOM, 7 (1955) 158.
[30] J. R. Groza, "Field–Activated sintering" in ASM Materials Handbook, vol. 7, p. 583 (ASM International, Materials Park, Ohio, 1998).
[31] High pressure field sintering apparatus, UC Davis, 2002.
[32] Cs. Balazsi, F. Gillemot, M. Horvath, F. Weber, K. Balazsi, F. Cinar Sahin, Y. Onuralp, A. Horvath, Structural Investigation of Nano-oxide Strengthened steels, J. Mater Sci, 46(13) (2011) 4598 – 4605.